2016

A Dielectric Rod Antenna for Picosecond Pulse Stimulation of Neurological Tissue

Ross A. Petrella
Old Dominion University, rpetr005@odu.edu

Karl H. Schoenbach
Old Dominion University, kschoenb@odu.edu

Shu Xiao
Old Dominion University, sxiao@odu.edu

Original Publication Citation

Petrella, R. A., Schoenbach, K. H., & Xiao, S. (2016). A dielectric rod antenna for picosecond pulse stimulation of neurological tissue. *IEEE Transactions on Plasma Science, 44*(4), 708-714. doi:10.1109/tps.2016.2537213

Published in final edited form as:

IEEE Trans Plasma Sci IEEE Nucl Plasma Sci Soc. 2016 April ; 44(4): 708–714. doi:10.1109/TPS.2016.2537213

A Dielectric Rod Antenna for Picosecond Pulse Stimulation of Neurological Tissue

Ross A. Petrella, **Karl H. Schoenbach**, and **Shu Xiao**

Frank Reidy Research Center for Bioelectrics, Department of Electrical and Computer Engineering, Old Dominion University, Norfolk, VA 23529, USA

Abstract

A dielectrically loaded wideband rod antenna has been studied as a pulse delivery system to subcutaneous tissues. Simulation results applying 100 ps electrical pulse show that it allows us to generate critical electric field for biological effects, such as brain stimulation, in the range of several centimeters. In order to reach the critical electric field for biological effects, which is approximately 20 kV/cm, at a depth of 2 cm, the input voltage needs to be 175 kV. The electric field spot size in the brain at this position is approximately 1 cm^2. Experimental studies in free space with a conical antenna (part of the antenna system) with aluminum nitride as the dielectric have confirmed the accuracy of the simulation. These results set the foundation for high voltage in situ experiments on the complete antenna system and the delivery of pulses to biological tissue.

Index Terms

Ultrawideband antennas; dielectric loaded antennas; picoseconds pulses

I. INTRODUCTION

Recent studies with high-voltage picosecond pulses showed that pulsed electric fields of just 20 kV/cm amplitude have strong effects on neurons. Hundred pulses at a repetition rate of 500 Hz caused membrane depolarization of neurons, which culminated in an action potential at injection currents of − 80 pA [1]. More recent studies on different cell types indicate that even a single pulse can cause an increase in cytosolic calcium. The results indicate that such picosecond pulses cause long-lasting opening of voltage gated calcium channels [2]. Whereas these studies were performed in vitro, with the electric fields generated between metal electrodes, the results indicate the feasibility of using wideband antennas for the delivery of such extremely short pulses to tissue, e.g. brain tissue over a distance of centimeters. While needle electrodes are typically used in this range, an antenna offers a noninvasive method to deliver pulses in vivo. The use of pulses with durations and/or rise-times on the order of 100 ps would allow us to focus the electric fields in subcutaneous tissue with a resolution in the subcentimeter range.

Efforts to utilize wideband antennas for the delivery of intense pulsed electric fields into tissue have led to the development of focusing wideband antennas [3,4]. For example the prolate spheroid impulse radiating antenna (PSIRA), a reflector type antenna for short distance illumination designed by Baum et al. [5,6], has the potential to generate large

electric fields in tissue. The electric fields produced by such reflector type antennas can be high enough to induce biological effects. Previously, using a parabolic impulse radiating antenna (IRA) designed for long distance scattering and feeding, pulses with a rise time of 200 ps and pulse width [full-width at half-maximum (FWHM)] of 400 ps, it is possible to generate a peak electric field of 68 kV/m at 10 m if the voltage fed into the antenna is 1 MV [7]. At closer distance, electrical fields in air could be much higher and close to the required field strength for biostimulation: 20 kV/cm. Yet, the electric field in biological targets is strongly reduced compared to that in air by the reflection at the interface of air and tissue, which is due to the large difference in permittivity. The relative permittivity of brain matter for example is approximately 50 at a frequency of 1 GHz [8]. As a result, the antenna-based delivery of subnanosecond electric pulses still has not found therapeutic applications.

An approach that can overcome the problem of losses at the interface of air and tissue is the use of a dielectric antenna. With such an antenna, the coupling of the radiation to the tissue can be strongly increased by making direct contact to the tissue. As will be shown, although it is not as efficient as large antennas, it permits the delivery of pulses to targets that are 1–2 cm in depth. Also, because the antenna is dielectrically loaded, it can be much smaller than a prolate-spheroidal antenna.

The dielectric antenna which is described in this paper consists of three sections: 1) a hollow conical TEM wave guide, which is loaded with a dielectric. Such a structure is commonly used for launching waves to a dielectric lens [9]. In principle it is an aperture antenna but has a small aperture area; 2) a dielectric rod, i.e., a cylindrical wave guide, which is used to confine the electromagnetic waves and guide them to the emitting section; and 3) a dielectric cone as the wave emitting section. The conical segment acts like a convex lens, confining the electric field to a small area and provides for the coupling of the dielectric interface between antenna and tissue, reducing reflections.

Such an antenna could be used to stimulate neurological tissue. We have therefore used CST Microwave Studio® to simulate the electric field distribution in a partial human head voxel model. The model consists of seven dielectrics with dielectric properties of skin, fat, bone, blood, optic nerve, and brain (grey and white matter). Aluminum Nitride (AlN) with $\varepsilon = 7.3$ was selected as the antenna dielectric material.

The performance of the antenna was examined with respect to: 1) the electric field orientation in the target tissue; 2) the electric field gradient (The electric field decreases as the wave penetrates, but the field at the skin covering the skull should not be excessively large compared to that in the target zone, so that damage can be avoided); 3) the spot size of the field confinement; 4) the magnitude of the electric field in the brain tissue. Since the critical electric field for inducing cell membrane permeabilization is approximately 20 kV/cm [1], we will assess how practical it is to reach such condition in the biological target. In order to verify the accuracy of the code, we have constructed and tested a dielectric antenna using a commercially off-the-shelf dielectric material (Aluminum Nitride ceramic).

II. ANTENNA DESIGN

The structure of the antenna is shown in Fig.1. It has three sections: the wave launching section, the dielectric wave guide, and the wave emitting section. The impulse source is connected to the apex of the wave launching section, so a TEM wave is formed and is further guided to the wave emitting section by the dielectric wave guide. Throughout the antenna, the same dielectric material is used. Unlike a typical antenna pointing to the free space, this antenna makes direct contact with a tissue through the dielectric cone in the wave emitting section. There is no air gap between the antenna and the tissue.

2.1 Section1: Wave Launching Section

In Section 1, two triangular metal plates are bent in a conical shape to symmetrically cover part of the dielectric cone. This part of the antenna is defined by two angles: the apex angle θ_0 and the azimuth angle ϕ_0. Such antenna was studied by Shen et al. [10]. The characteristic impedance of the wave launching section is:

$$Z_0 = \frac{Z_c}{2\sqrt{\varepsilon_r}} \frac{K(\cos\phi_0)}{K(\sin\phi_0)} \quad (1)$$

where,

$$K(\sin\phi_0) = \int_0^{\pi/2} \frac{d\beta}{\sqrt{1 - \sin^2\varnothing_0 \sin^2\beta}}$$

$$K(\cos\phi_0) = \int_0^{\pi/2} \frac{d\beta}{\sqrt{1 - \cos^2\varnothing_0 \sin^2\beta}}$$

Z_c is the free space impedance (377 Ω)and ε_r is the dielectric permittivity of the dielectric. For the dielectric we studied, Aluminum Nitride ceramic (ε_r = 7.3), the characteristic impedance is shown in Fig.2. This allows us to identify the angle of ϕ_0 for a given impedance.

The important features of an infinitely long version of this antenna (consisting of only wave launching section) are: 1) frequency independence (important for wide-band pulses) 2) uniform azimuthal directivity and 3) TEM mode excitation. However, we have to deal with an antenna that has a finite length, which can be as short as a few centimeters. The scattering of the electromagnetic waves at the end of the conical transmission line will in this case cause pulse ringing or pulse broadening at the target. This corresponds to the increase in pulse duration at the target. This may be unfavorable for radar or communication applications, but for biological applications it may be useful since the threshold electric fields for biological effects generally is reduced as the pulse duration increases, thus easing the requirement of the pulsed power system.

2.2 Section 2: Dielectric Wave Guide

Dielectric wave guides are commonly used for guiding high frequency electromagnetic waves, such as millimeter waves and light waves. While many modes of waves can propagate in the cylindrical wave guide, the fundamental mode (lowest) is HE_{11} mode, for which the cutoff frequency is very low. As such, wideband signals are favored [11]. Outside the waveguide, an evanescent wave propagates with the speed of light in free space, but the field intensity decreases exponentially in radial direction from the waveguide surface. So the wave energy is mostly confined in the dielectric wave guide.

When determining the diameter of the rod, a rule of thumb is that the radius R should be greater than the pulse spatial width:

$$R > \frac{t_p c_0}{\sqrt{\varepsilon_r}} \quad (2)$$

where t_p is the pulse duration. This means that the pulse reflected from the rod-air interface will be temporally separated from the existing pulse on the axis. The axis is the location of the highest power density, and consequently the pulse is defined mainly by the waves on the axis. For small radius rods, the reflection adds to the existing pulse temporally, creating distorted waveforms. This distortion is pronounced for low frequency waves or long pulses. Therefore, the radius essentially determines the low frequency limit of the antenna.

As far as the length of the dielectric wave guide L concerns, it should satisfy (Fig.3):

$$\left(\frac{R}{\sin\theta_0} + \sqrt{R^2+L^2} - \frac{R}{\tan\theta_0} - L\right)\frac{\sqrt{\varepsilon_r}}{c_0} > t_p \quad (3)$$

This condition ensures the pulse will not be broadened once it reaches the end of the wave guide. Waves scattered off at the discontinuity at the interface from the dielectric rod to the air also contribute to the pulse duration if they reach the end of the wave guide at the same time and cause a broadening of the pulse.

2.3 Coupling of Wave Launching Section with Dielectric Wave Guide

At the intersection of the conical wave launching section with the cylindrical wave guide (Section 2), the incident waves should ideally be reflected towards the axis of the cylindrical wave guide. This can be achieved using the concept of total internal reflection. The critical angle for total internal reflection is:

$$\beta_0 = \sin^{-1}\left(\frac{1}{\sqrt{\varepsilon_r}}\right) \quad (4)$$

with ε_r being the relative permittivity of the dielectric and with β_0 being the complementary angle to the apex angle (Fig. 4).

When Eq. 4 is applied to dielectrics with large permittivity, the result is a relatively small β_0 and consequently a large θ_0. For example, $\beta_0 = 21°$ for $\varepsilon_r = 7.3$. Such a configuration, where the wave launching section is rather short is undesirable. This is because the waves propagating at angles $\theta < \theta_0$ in the wave launching section will arrive at Section 2 earlier than those where θ is close to θ_0 (see Fig.4, dashed line). Consequently, at the interface of Section 1 and Section 2 the wave front is still spherical. In order to preserve the pulse shape of the incident pulse in the cylindrical wave guide, the incident waves Section 2 should ideally be planar waves. However this can only be achieved by using a small slope launcher (large β_0 and small θ_0), which resembles to some degree two parallel plates.

It seem that keeping the wave launching section short (large θ_0) has certain advantages such as low losses due to scattering and high axial electric fields in the rod. However, that needs to be balanced against the distortion of the waves. Considering the importance of preserving the pulse shape in the antenna it might be still preferable to use a wave launcher with a small apex angle.

2.4 The Electric Field on the Axis

The electric field radiated from the wave launcher can be obtained from the aperture theory [12]. Given the coordinate system seen in Fig. 1, the tangential component of the electric field on the aperture plane is known [10], the radiated field at a point on the axis is:

$$\mathrm{E_y}\left(\overrightarrow{R_0}, t\right) = \mathrm{E_0}\{\alpha^{(1)}_{\mathrm{y,y}} \frac{\mathrm{a}^2}{\mathrm{R_0 c}} \frac{\partial}{\partial \mathrm{t}} \mathrm{f}\left(\mathrm{t} - \frac{\mathrm{R_0}}{\mathrm{c}}\right) + \alpha^{(2)}_{\mathrm{y,y}} \frac{\mathrm{a}^2}{\mathrm{R_0^2}} \mathrm{f}\left(\mathrm{t} - \frac{\mathrm{R_0}}{\mathrm{c}}\right)\} \quad (5)$$

where R_0 is the distance of an observer on the axis from the aperture center. The input pulse has a time dependence of f(t), but for the observer the pulse has a propagation delay $t - R_0/c$. For the near field, this delay is negligible. The field depends on both the input pulse voltage and the time derivative of the pulse. Specifically, for the field term near the antenna, f(t) is dominant and the time derivative term $\partial f(t)/\partial t$ is dominant for the field far from it. The coefficients $\alpha^{(1 \text{ or } 2)}_{y,y}$ depict the integral of the tangent electric fields over the aperture plane. In general, homogenous unidirectionally aligned “currents” resulting from a uniform illumination produce larger coefficients and hence larger electric fields. In this case, a low impedance conical wave launcher (correspondingly large ϕ_0) is preferable for radiating waves at high intensity. The aperture size preferably is comparable to the observing distance, so the ratios of $\alpha^{(1 \text{ or } 2)}_{y,y}$ over R_0 or R_0^2 are not small, which means that the ratio of L/R should not be too large.

2.5 Section 3: The Wave Emitting Section

The purpose of the third section of the antenna is to radiate the electric field into the tissue. Applying the ray theory, the dielectric taper refracts the incident waves and directs them towards the apex. In this way the terminal taper acts like an axicon with a majority of the energy entering the tissue near the apex.

The impinging ray should be reflected at the surface of the cone and then exit from the cone apex. This requires the angle of the cone to be α_0, the critical angle for total internal reflection (Fig.5):

$$\alpha_0 = \sin^{-1}\left(\frac{1}{\sqrt{\varepsilon_r}}\right) \quad (6)$$

This ensures the rays that are in parallel with the axis reach the cone apex and radiate into the tissue. For fields scattered off at the end of the wave launcher, the incident angle, α, can be larger than α_0. They are still totally reflected, but the reflected waves create focal points inside the cone, rather than reaching the cone apex. When α is less than α_0 refraction occurs and the transmitted wave departs the cone and becomes spread around the cone apex. This causes a widening of the focal spot in the tissue.

III. RESULTS

3.1 Antenna Parameters

The wave launcher (Section 1) was designed to use with a commercially available dielectric material, AlN (ε_r = 7.3), and to have an impedance of 50 Ω. Using these criteria, the azimuth angle ϕ_0 was determined to be 62.95° according to Eq.1 and Fig.2. For a pulse width of 100 ps, the diameter of the rod, which equals to the base diameter of the wave launcher, can be determined from Eq. 2, as R > 1.11 cm. Consequently a radius of 1.5 cm was chosen. For θ_0 we chose an angle of 29°. The length of Section 2 was set to be twice the value of R, 3 cm. Finally, the angle of the cone α_0 in antenna's Section 3 was calculated to be 21°. These parameters were used as initial values for the CST model, but have in the following been optimized using CST studio's Trust Region Framework optimization algorithm. The goal of the optimization was to maximize the electric field inside the brain tissue at a depth of 20 mm.

At the apex of cone, the pulse with Gaussian waveform and an amplitude of 1 V was applied (0–5 GHz). The antenna was applied to a CST partial head voxel model with a resolution of $1 \times 1 \times 1$ mm^3. The target was organized into layers comprised of 1 mm of skin, 5 mm of fat, 8 mm of bone, 1–10 mm of nervous opticus, and at least 50 mm of intermingled grey and white matter. Their respective electrical properties were provided by CST studio.

The three parameters for optimization were the rod diameter (R), rod length (L), and the taper angle (α). The resulting geometry can be seen in Fig. 6. The dielectric rod had a radius of 30 mm and a height of 35 mm. For the wave emitting section, the angle α was 10°.

3.2 Simulation Results

The wave launched from the apex is guided to the emitting section, as shown in several snap shots (Fig.7). The electric field travels down the wave launching section in a spherical wave form at 0.75 ns. The pulse is scattered at the joint between Section 1 and Section 2. Three scattered waves can be clearly observed at 1 ns: a reflected wave which bounces back to the source, an evanescent wave on the rod surface, and the waves confined in the rod. The last

part refracts into the brain tissue at 1.25 ns and reaches the brain tissue at 2 cm depth at 1.5 ns.

The performance of the antenna was assessed in terms of the electric field orientation, spot size, and magnitude. The electric field orientation at the 2-cm deep layer can be seen in Fig. 8. The electric fields were clamped at the values greater than 90% of the maximum value in the brain tissue for an easy observation. In general, the field is oriented in the −y direction. It is confined to the area projected straight down from the apex of the dielectric rod. Inside the brain tissue the electric field lines are approximately linear and run parallel to the skin-wave launcher interface. The maximum fields are concentrated in the area directly underneath the center of the wave launcher. It is desirable to have such linearly oriented fields in the confined region. This is a similar field structure to that obtained with the parallel plate electrodes and allows us to compare results obtained in vitro with those expected by this antenna.

If we define the stimulation spot size as the area that has an electric field value greater than 90% of the peak value, the thickness and width of the stimulation spot can be estimated to be 5 mm by 11 mm (Fig.7). At the surface the spot size is on the order of the diameter of the waveguide and shrinks until reaching 11 mm in width in the brain tissue (2 cm deep). This field concentration is caused by the tissue attenuation. Since the electric field is highest at the center and it remains to be so at deeper regions in the brain. (Fig.9).

The peak values of the pulse waveforms are plotted versus depth (Fig.10). It shows that as the depth increases the peak electric field decreases. The electric field in the brain tissue is approximately 42% of that at the skin surface. In terms of absolute field, the peak field in the brain is 11.5 V/m for a 1 V input. This implies that skin tissue may need to tolerate a field level 2–3 times as that of a brain tissue. Using 20 kV/cm as a threshold for a biological effect [1], a 175 kV pulse power supply would be required.

3.2 Experimental Results

To experimentally verify the results of voxel model, artificial tissue stimulants of skin, bone and brain can be used and a receiving antenna can be embedded in the tissue for measuring electric fields at various positions, similar to that described in [5]. While this experiment is still under preparation, we report on the validity of the modeling results by constructing a conical antenna and measuring the electric field in free space. The antenna was designed as 200 Ω and only has Section 1, i.e., the wave launcher. The two triangular metal plates that make up the wave launching section were adhesive copper foil with an azimuth angle ϕ_0 = 2.5°. The antenna has AlN (ε = 7.3) as the dielectric material and is constructed with a base diameter of 20 mm and height of 36 mm. The antenna was driven by a FID pulse generator (FID) through a 1:4 balun (50 Ω: 200 Ω). It was mounted in the upright direction. To measure the field on the vertical axis, a Prodyn AD-80(R) D-dot sensor was used. The setup is shown in Fig.11. We note that the sensor is a differential probe that has a ground plane which was aligned to the mid-plane of the conical antenna. The effective area of the D-dot sensor is in the emissive probe with an area of 3×10^{-4} m^2. The probe was aligned with the axis of the conical antenna. By adjusting the vertical position, we were able to measure the

field distribution in the free space. The signal was integrated on the oscilloscope to obtain the electric field.

The measured electric field and the simulated result are shown in Fig.11. The two waveforms (Fig.11b) are almost identical at times of less than 2.7 ns, but a difference occurs afterwards. This is due to the wave scattering on the holder and desk, which is not included in the simulation. When the peak of the electric field was sampled on the axis, Fig.12 shows the results obtained from Eq.2 (analytical), the simulation and from the measurements. The three results are very close, except at the distance of less than 40 mm: here the measurement results are slightly lower than the modeled and calculated values. In this case, the error could be caused by the finite size of the effective biconical area of the probe. The field across the probe is not homogenous when the probe is close to the antenna aperture. As the distance from the antenna aperture increases, such distortion becomes diminished so the results are almost identical to the simulation and analytical results. Overall, the results of these experimental studies indicate that the results obtained for human voxel model can serve as a guide for the future experiments in tissue.

IV. CONCLUSIONS

In a simulation, electric pulses in the hundred picosecond range were successfully delivered to the subcutaneous region of the brain using a conical dielectrically loaded antenna. The antenna makes a direct contact to the tissue, without air gap, thus reducing the large reflection losses due to the difference in the permittivity of air and tissue. For the dielectrically loaded antenna ($\varepsilon = 7.3$), the electric field at a depth of 20 mm (inside brain tissue) was shown to be 11.5 V/m for a 1V input. In order to stimulate tissue, the critical electric field needs to be on the order of 20 kV/cm, as found in our previous study [1]. This critical field corresponds to an input voltage of 175 kV. This voltage is achievable with current pulsed power systems. The spot size in the brain is estimated to be 5 mm × 11 mm × 11 mm and is better than that created by other neural stimulation modalities, specifically repetitive transcranial magnetic stimulation (rTMS) [13]. For this spot volume, the electric field at the skin is 2.4 times greater than the field in the brain tissue. The model used in this study was validated by comparing the modeling results with experimental results. The results obtained in free space suggest that the antenna simulation is reliable and can provide a solid ground for the necessary experiments to confirm the utility of the complete dielectrically loaded antenna in biological tissue. The tissue type is not limited to neurological tissue but can also be used for superficial targets such as skin or tissues in culture.

Acknowledgments

This project was sponsored by NIH with a R21 project (1R21EB016912-01A1).

References

1. Xiao S, Pakhomov A, Gou F, Polisetty S, Schoenbach K. Neurostimulation using subnanosecond electric pulses. Progress in Biomedical Optics and Imaging: Terahertz and Ultrashort Electromagnetic Pulses for Biomedical Applications. 2013 Feb.14(21)

2. Semenov I, Xiao S, Kang D, Schoenbach KH, Pakhomov AG. Cell stimulation and calcium mobilization by picosecond electric pulses. Bioelectrochemistry. 2015; 105:65–71. [PubMed: 26011130]
3. Baum CE. Focal waveform of a prolate- spheroidal impulse-radiating antenna. Radio Science. 2007; 42:RS6S27.
4. Xiao S, Altunc S, Kumar P, Baum CE, Schoenbach KH. A reflector antenna for focusing in the near field. IEEE Antennas and Wireless Propagation Letters. 2010 Mar.9:12–15.
5. Kumar P, Baum CE, Altunc S, Buchenauer J, Xiao S, Christodoulou CG, Schamiloglu E, Schoenbach KH. A hyperband antenna to launch and focus fast high-voltage pulses onto biological targets. IEEE Trans. Microwave Theory and Techniques. 2011 Apr; 59(4):1090–1101.
6. Guo F, Yao C, Bajracharya C, Polisetty S, Schoenbach KH, Xiao S. Simulation of delivery of subnanosecond pulses to biological tissues with impulse radiating antenna. Bioelectromagnetics. 2013 Nov 6.
7. Prather WD, Baum CE, Torres RJ, Sabath F, Nitsch D. Survey of worldwide high-power wideband capabilities. IEEE Trans. Electromagnetic Compatibility. 2003; 46(3):335–344.
8. Foster KR, Schepps JL, Stoy RD, Schwan HP. Dielectric properties of brain tissue between 0.01 and 10 GHz. Phys Med Biol. 1979 Nov; 24(6):1177–1187. [PubMed: 531093]
9. Baum CE. Emerging technology for transient and broad-band analysis and synthesis of antennas and scatterers. Proc. IEEE. 1976; 64(11):1598–1616.
10. Shen HM, King RWP, Wu TT. V-conical antenna. IEEE Trans Antennas Propagat. 1988 Nov; AP-36(11):1519–1525.
11. Balanis, CA. Advanced Engineering Electromagnetics. 2nd. Wiley; 2012.
12. Baum CE. Focused aperture antennas. Sensor and Simulation Notes. 1987 Note 306.
13. Deng Z, Lisanby SH, Peterchev AV. Electric field depth–focality tradeoff in transcranial magnetic stimulation: simulation comparison of 50 coil designs. Brain Stimulation. 2013; 6(1):1–13. [PubMed: 22483681]

Biographies

Ross A. Petrella received his B.S in Biomedical Engineering from Virginia Commonwealth University, Richmond, VA in 2014. He is currently a Ph.D student in Biomedical Engineering at Old Dominion University in Norfolk, Va. His research interests include electromagnetic effects on cells and the design of systems to deliver electromagnetic energy to biological targets.

Karl H. Schoenbach (F’94, LF’12) is an Eminent Scholar Emeritus and Professor Emeritus of Electrical and Computer Engineering at Old Dominion University in Norfolk, VA. He held the Batten Endowed Chair in Bioelectric Engineering and served as founding director of the Frank Reidy Research Center for Bioelectrics. His research efforts reached from basic

research on electrical discharges in gases and liquids to environmental and medical applications of pulse power technology. He has published more than 200 papers in peer-reviewed journals, many of them on biological effects of ultrashort electrical pulses, and his work is cited more than 14,000 times with an h-index of 62.

Shu Xiao (M’02-SM’14) received the Ph.D. degree in electrical engineering from Old Dominion University, Norfolk, VA, in 2004. He was in the MS/PhD joint program in the University of Electronic Sciences and Technology of China, Sichuan, from 1996 to 2001. He is currently Associate Professor in the Department of Electrical and Computer Engineering, Old Dominion University, where he teaches power electronics and electric drives. His research interests include pulsed power, high power electromagnetics, electrical discharges in liquids and gases. His research also includes using pulsed power and pulsed electromagnetic radiation in biomedical applications.

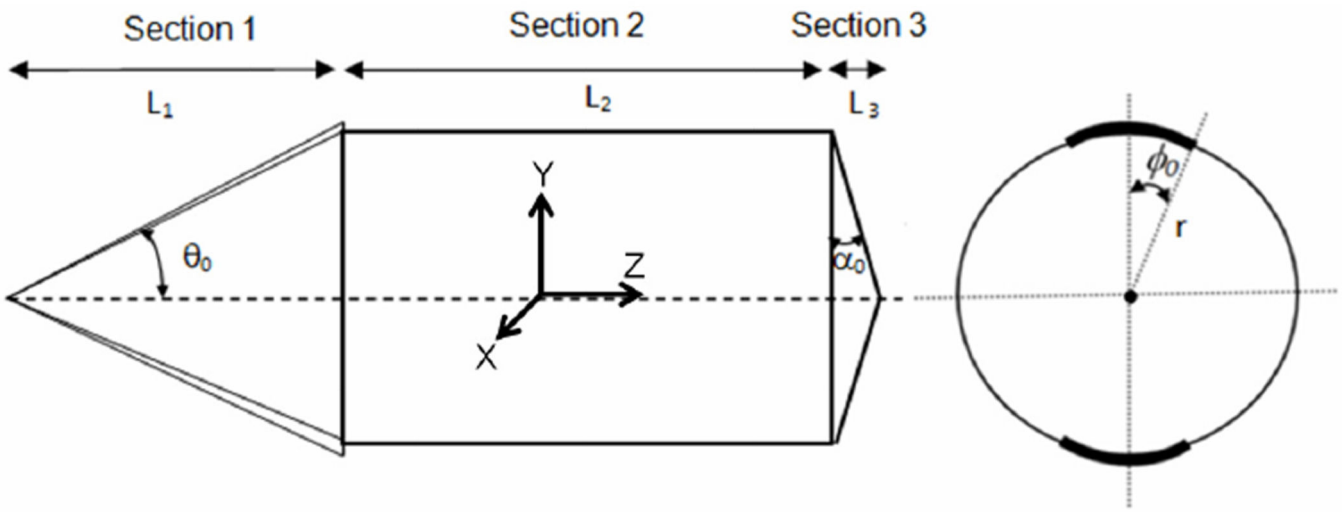

Fig. 1.

A conical antenna that is loaded with a dielectric. In Section 1, the wave is launched by a conical waveguide centered on the y axis and is characterized by two angles: θ_0 and ϕ_0. In Section 2, the waves emitted from the launching section are guided by a dielectric rod to the emitting section. In Section 3, the waves are detached from the antenna and propagate in the +z direction.

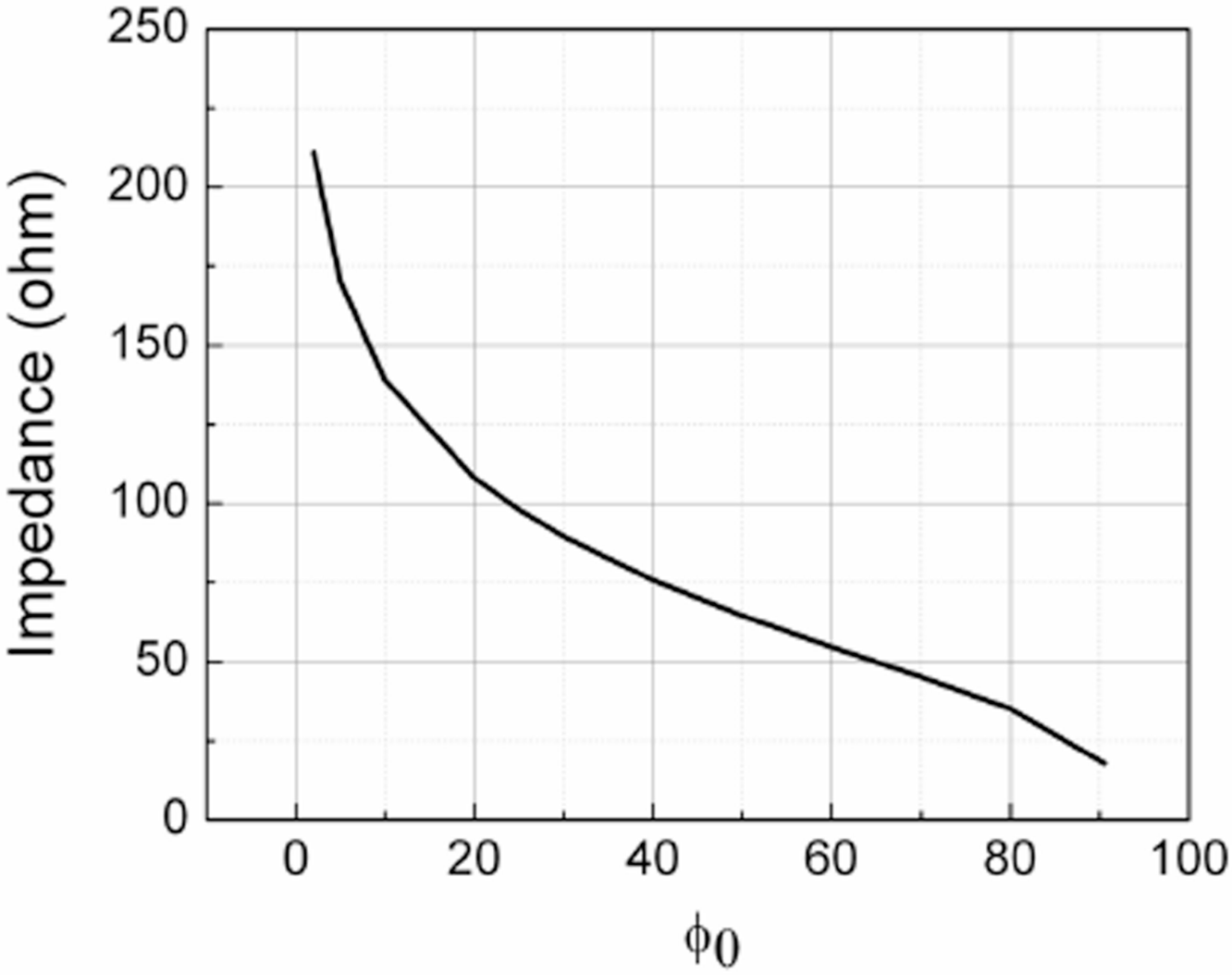

Fig. 2.
The characteristic impedance of a conical antenna loaded with Aluminum Nitride.

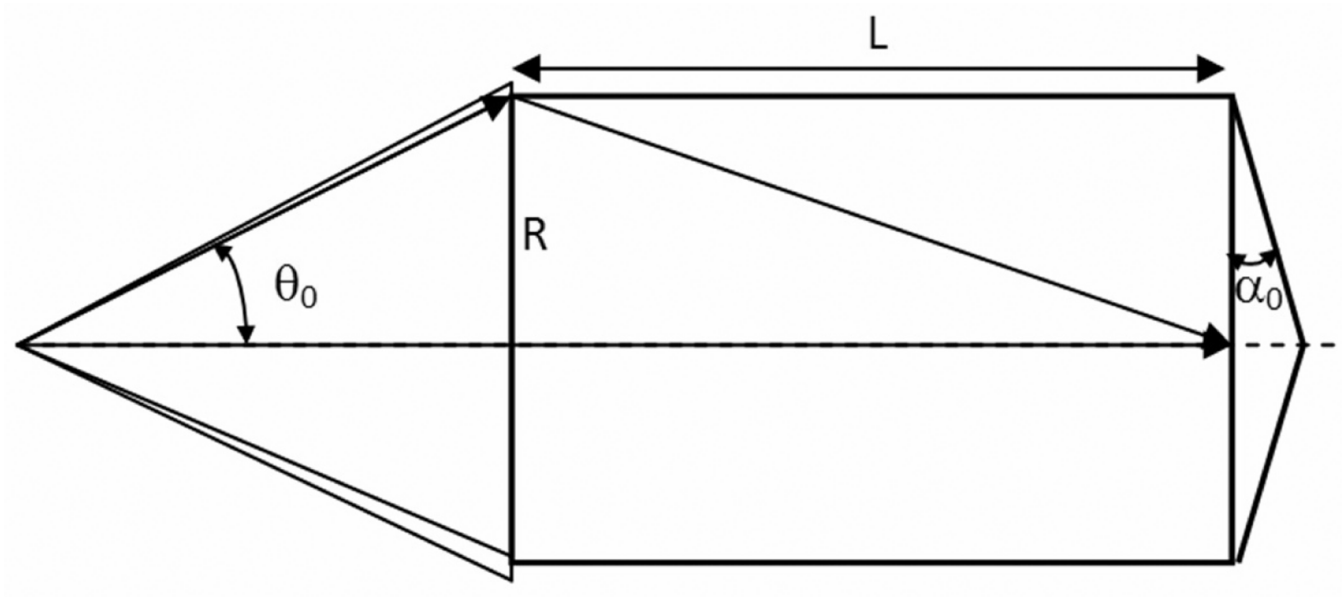

Fig. 3.

The radius (R) and the length of the dielectric wave guide (L) should ensure the clear separation of wave directly reaching the end of the wave guide from that scattered off at the discontinuity between the conical wave guide and the dielectric wave guide.

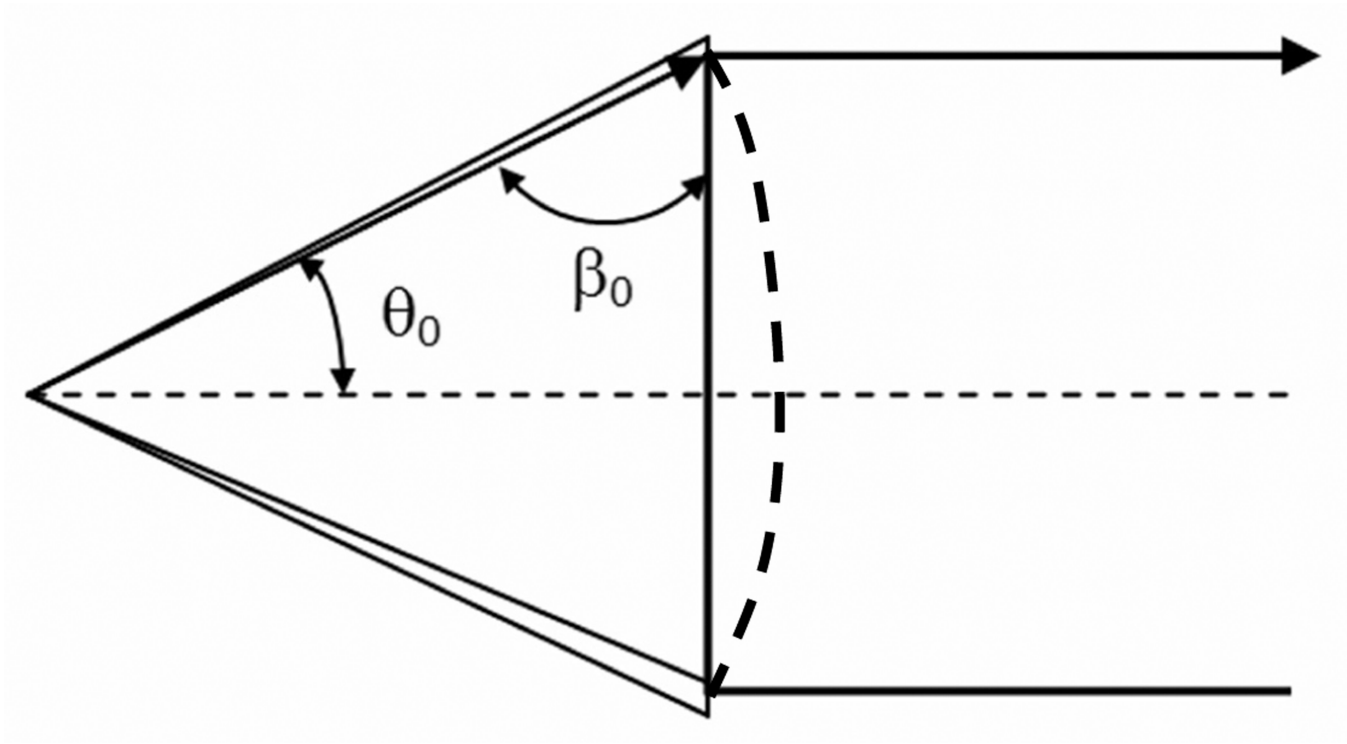

Fig. 4.

The critical angle for total internal reflection applies to the wave when it is guided by a conical wave guide. The dielectric constant is ε_r.

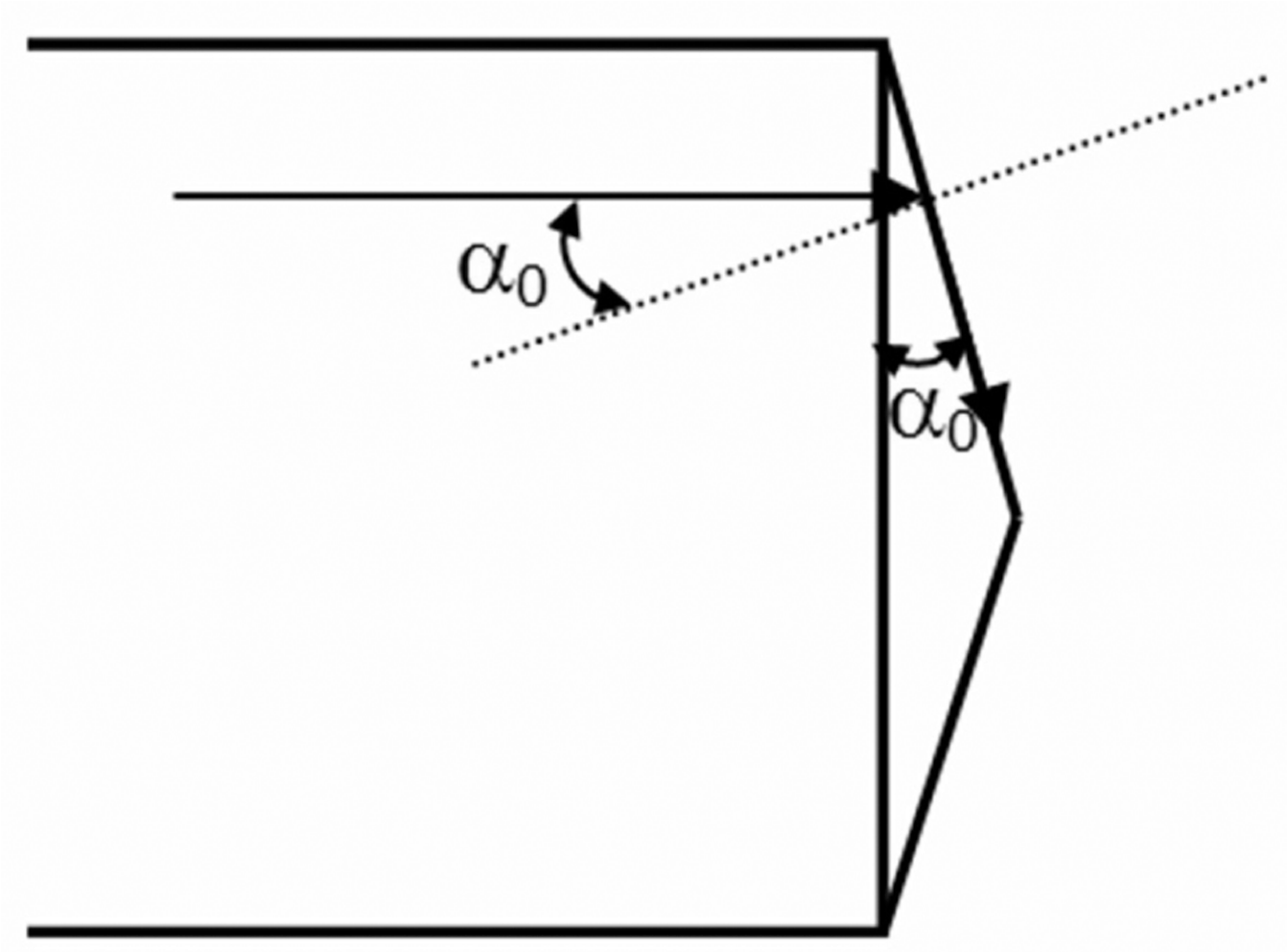

Fig. 5.
A conical antenna that has a cone as the emitting section.

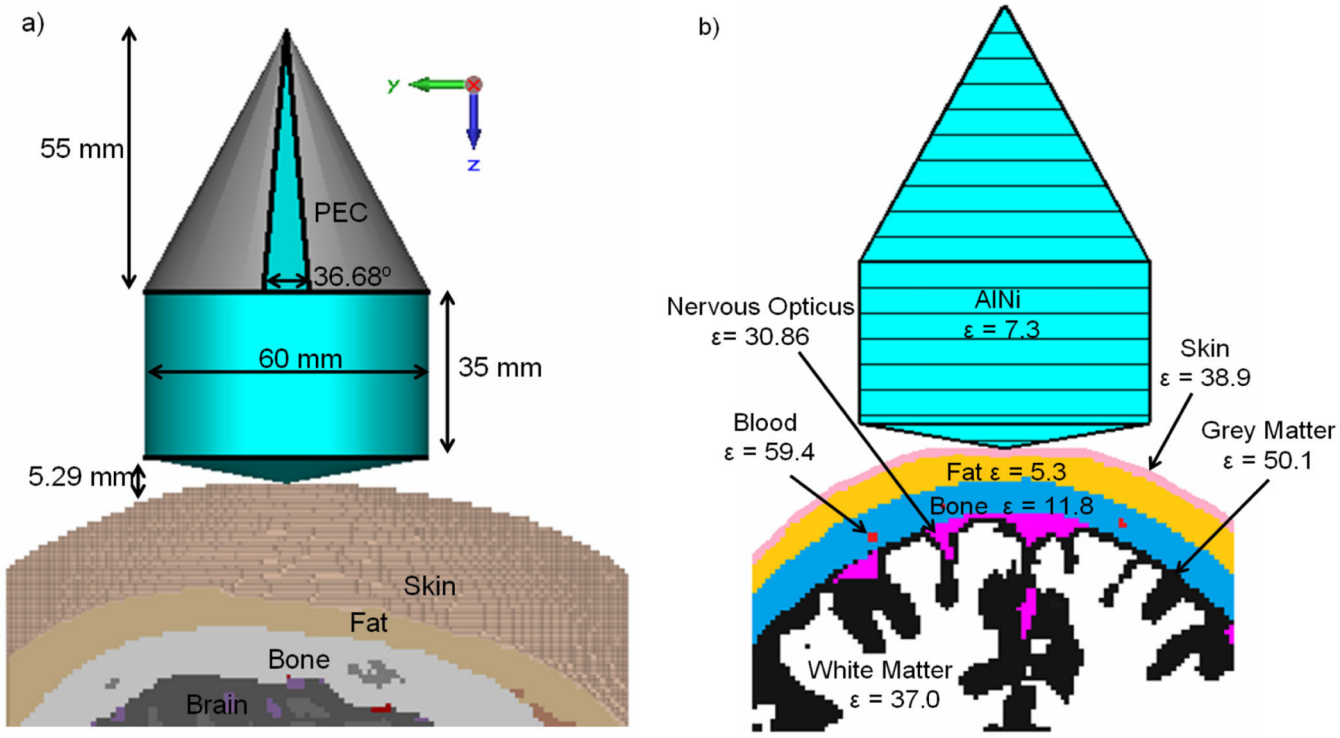

Fig. 6.

a) The optimized CST Studio model with dimensions sitting on the voxel model target. b) A cross sectional view of the model and target showing the materials and their respective permittivity.

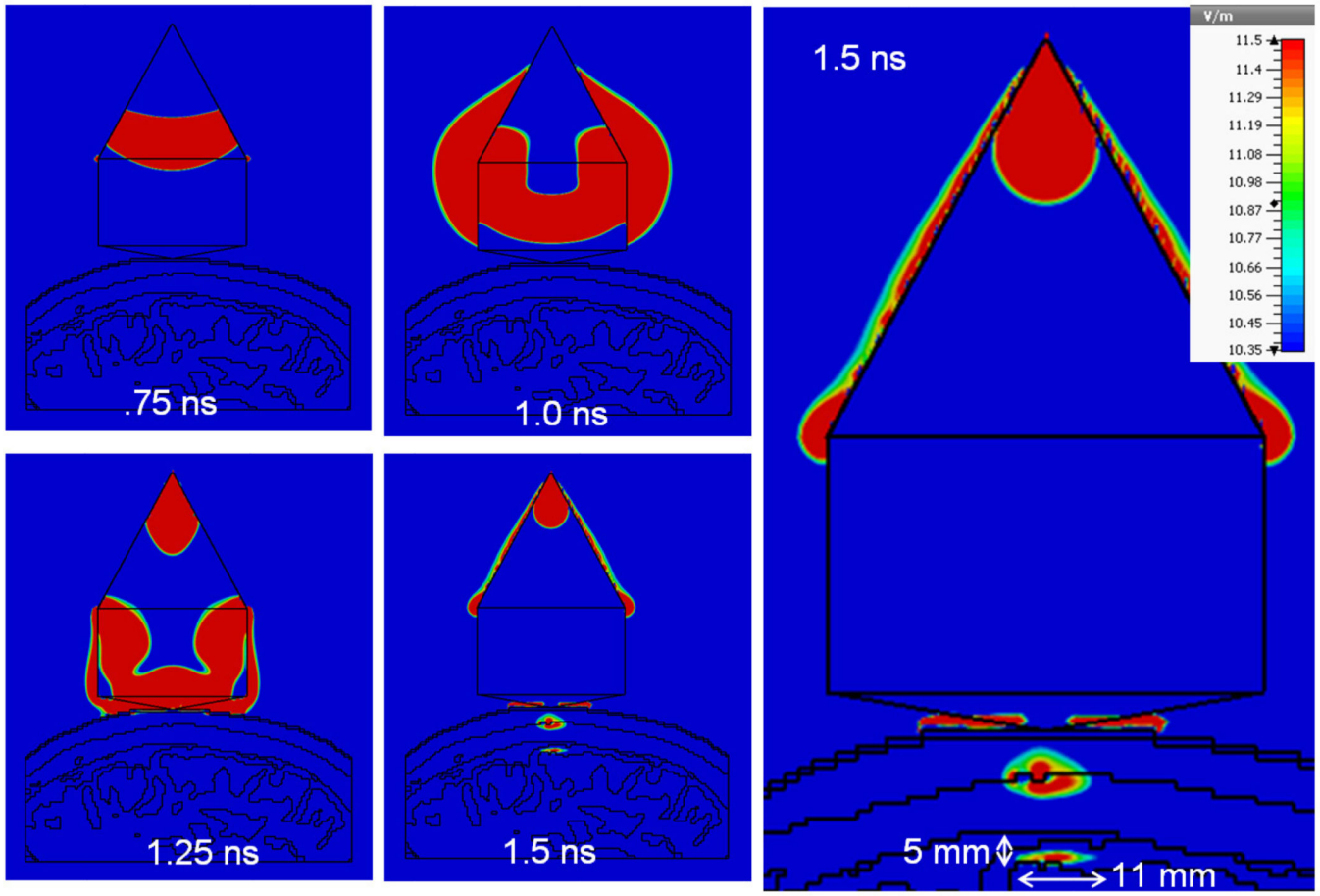

Fig. 7.

The transient propagation of the electric field shows an excitation of the brain tissue at 11.5 V/m with a diameter of approximately 11 mm.

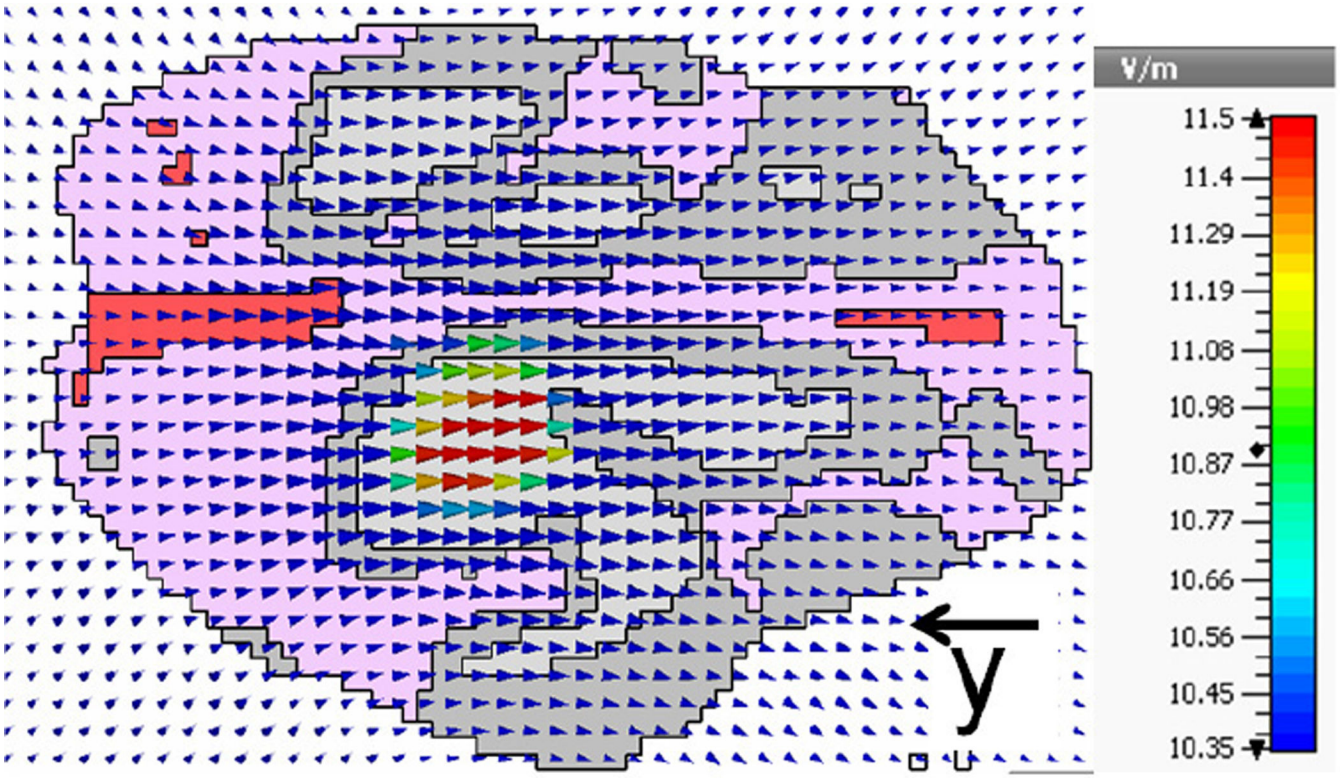

Fig. 8.

The electric field is linearly oriented inside the brain tissue. The size of the arrow indicates the intensity of the electric field.

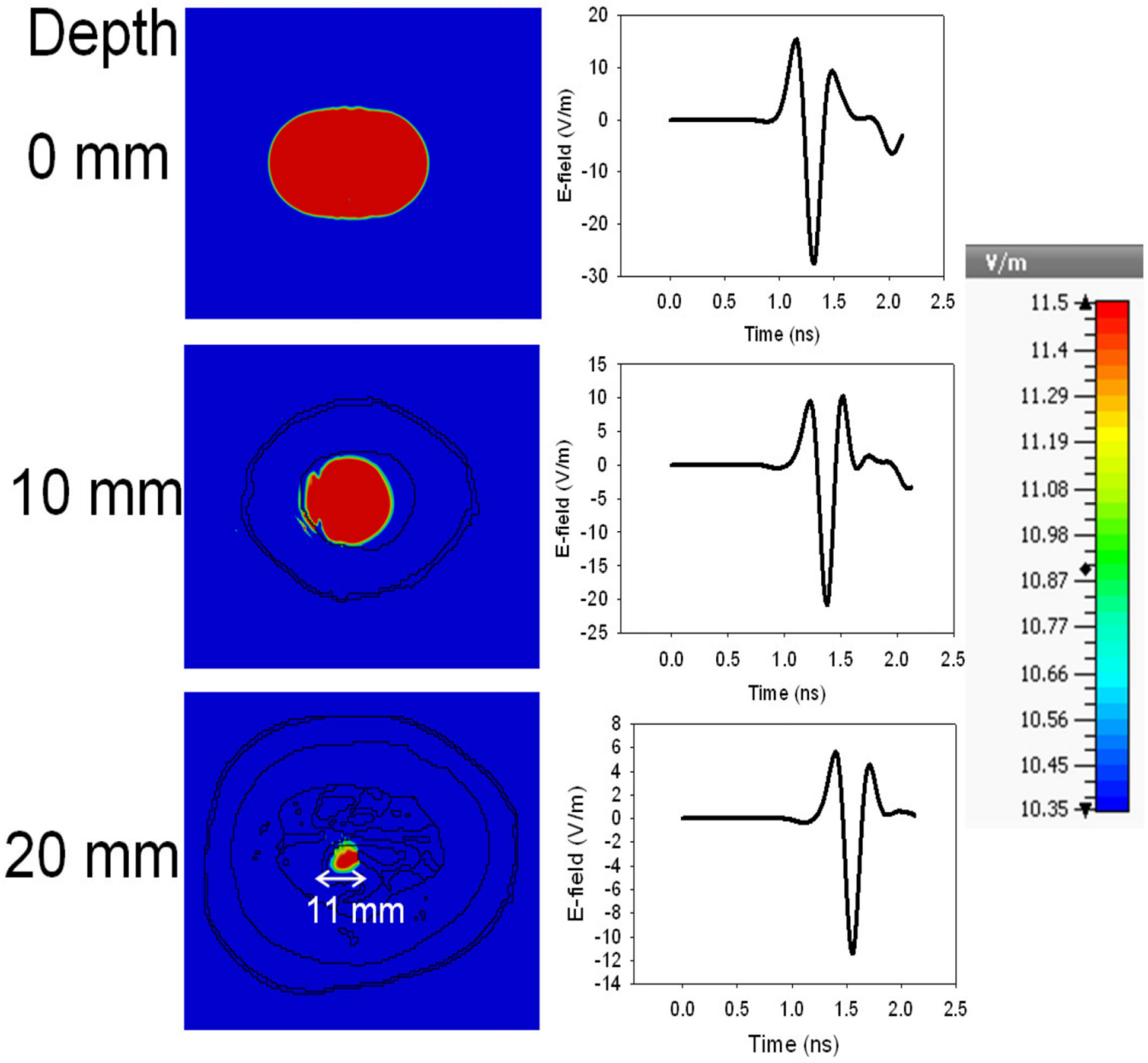

Fig. 9.

Cross sectional view of the brain tissue at three depths shows the field decreasing in magnitude and size with increasing depth.

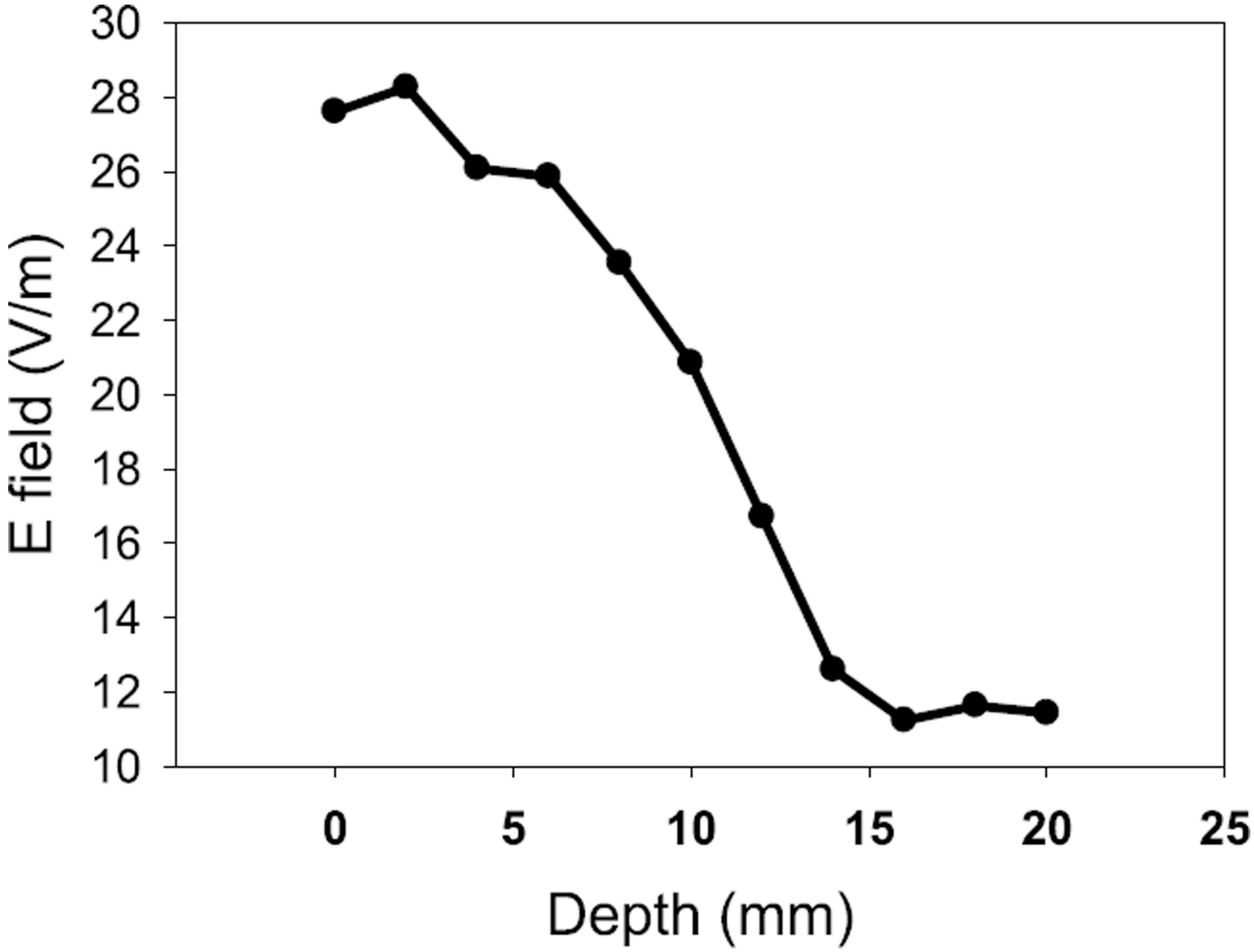

Fig. 10.

The electric field distribution from the skin to the brain. The electric field magnitude decreases from 27.6 V/m at the skin surface and reaches 11.5 V/m inside the brain tissue.

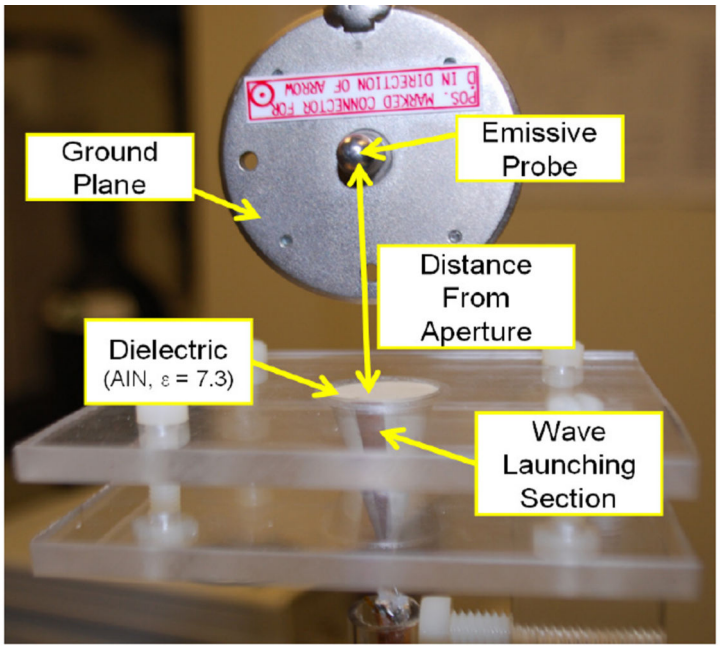

(a)

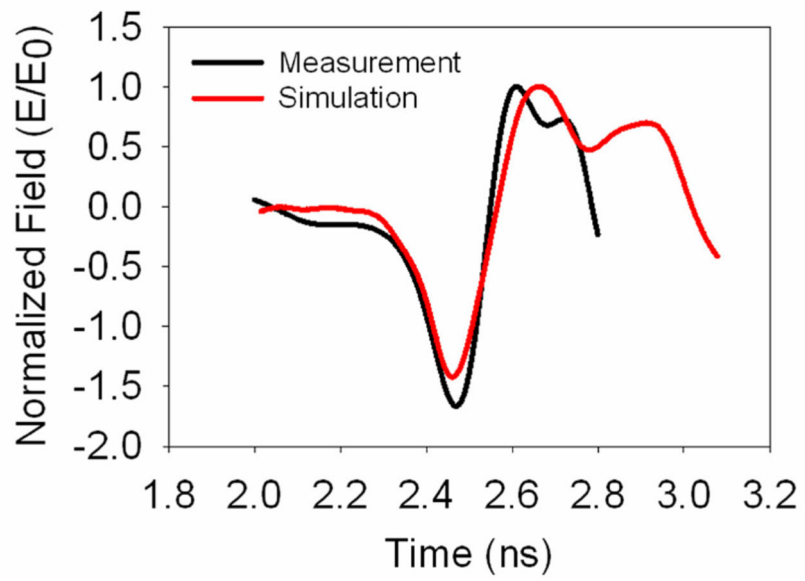

(b)

Fig. 11.

The experimental setup in free space. a) A conical antenna with a characteristic impedance of 200 Ω was tested. The receiver is a D-dot sensor (Prodyn AD-80 (R)). b) The waveforms of the simulation and measurement.

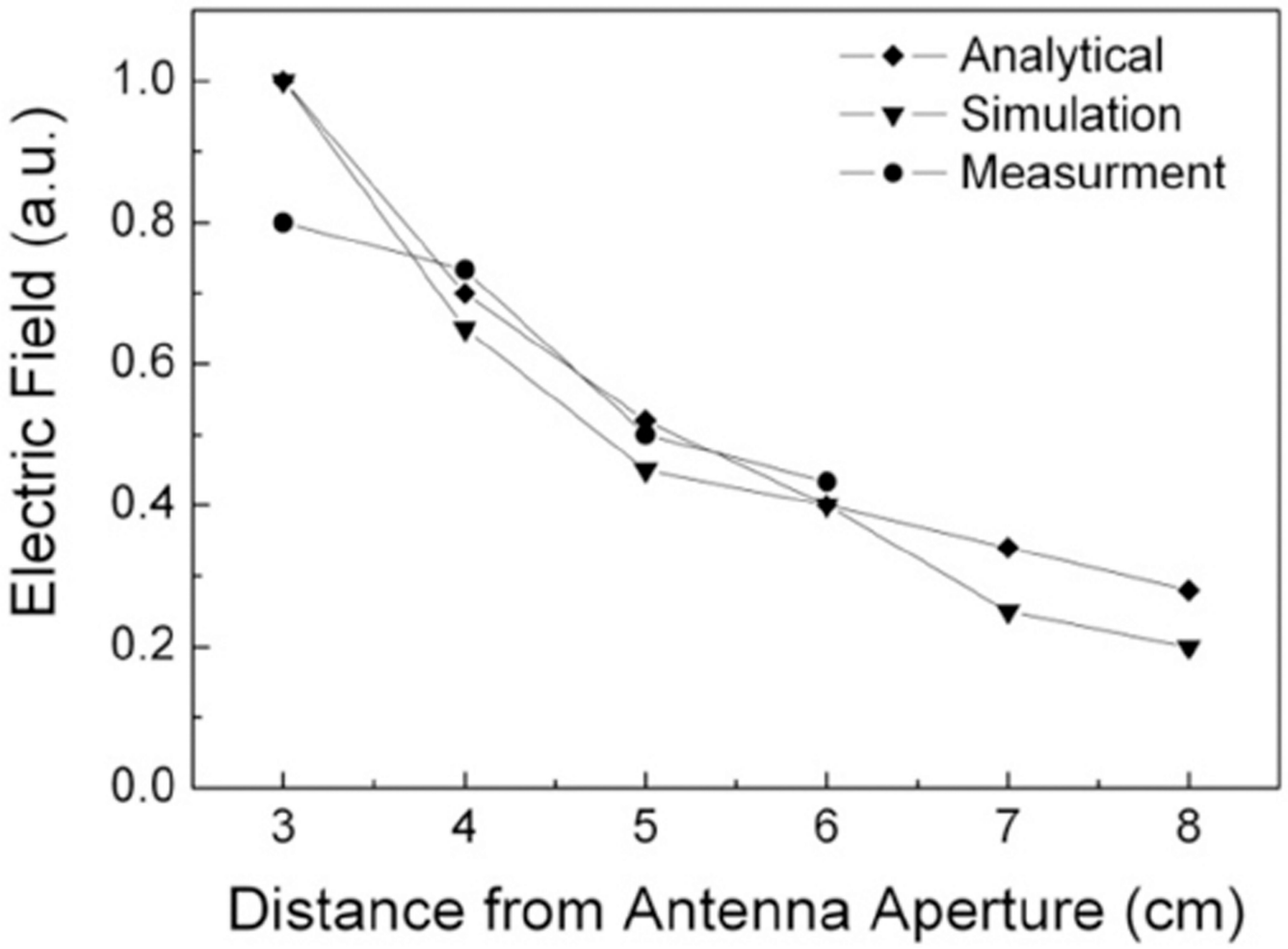

Fig. 12.
The electric field distribution for a 200 Ω conical antenna. Measurement results, simulated results and the analytical results from Eq.2 are shown.